tvst

Cornea & External Disease

Detection of TTR Amyloid in the Conjunctiva Using a Novel Fluorescent Ocular Tracer

Julie Pilotte[1], Alex S. Huang[2], Sami Khoury[1], Xiaowei Zhang[2], Ali Tafreshi[1], Peter Vanderklish[1], Stella T. Sarraf[1], Jose S. Pulido[3], and Tatyana Milman[3,4]

[1] Amydis, Inc., La Jolla, CA, USA
[2] Hamilton Glaucoma Center, Shiley Eye Institute, Viterbi Family Department of Ophthalmology, University of California San Diego, La Jolla, CA, USA
[3] Vickie and Jack Farber Vision Research Center and MidAtlantic Retina Service, Wills Eye Hospital, Philadelphia, PA, USA
[4] Pathology Department, Wills Eye Hospital, Philadelphia, PA, USA

Correspondence: Tatyana Milman, Pathology Department, Wills Eye Hospital, 840 Walnut Street, Suite 1410, Philadelphia, PA 19107, USA.
e-mail: tmilman@willseye.org

Received: August 15, 2023
Accepted: December 15, 2023
Published: February 15, 2024

Keywords: Transthyretin amyloidosis; ocular and periocular tissues; Conjunctival TTR deposits

Citation: Pilotte J, Huang AS, Khoury S, Zhang X, Tafreshi A, Vanderklish P, Sarraf ST, Pulido JS, Milman T. Detection of TTR amyloid in the conjunctiva using a novel fluorescent ocular tracer. Transl Vis Sci Technol. 2024;13(2):11, https://doi.org/10.1167/tvst.13.2.11

Background: Transthyretin amyloidosis (ATTR) is a significant cause of cardiomyopathy and other morbidities in the elderly and Black Americans. ATTR can be treated with new disease-modifying therapies, but large shortfalls exist in its diagnosis. The objective of this study was to test whether TTR amyloid can be detected and imaged in the conjunctiva using a novel small-molecule fluorescent ocular tracer, with the implication that ATTR might be diagnosable by a simple eye examination.

Methods: Three approaches were used in this study. First, AMDX-9101 was incubated with in vitro aggregated TTR protein, and changes in its excitation and emission spectra were quantified. Second, a cadaver eye from a patient with familial amyloid polyneuropathy type II TTR mutation and a vitrectomy sample from an hATTR patient were incubated with AMDX-9101 and counterstained with Congo Red and antibodies to TTR to determine whether AMDX-9101 labels disease-related TTR amyloid deposits in human conjunctiva and eye. Last, imaging of in vitro aggregated TTR amyloid labeled with AMDX-9101 was tested in a porcine ex vivo model, using a widely available clinical ophthalmic imaging device.

Results: AMDX-9101 hyper-fluoresced in the presence of TTR amyloid in vitro, labeled TTR amyloid deposits in postmortem human conjunctiva and other ocular tissues and could be detected under the conjunctiva of a porcine eye using commercially available ophthalmic imaging equipment.

Conclusions: AMDX-9101 enabled detection of TTR amyloid in the conjunctiva, and the fluorescent binding signal can be visualized using commercially available ophthalmic imaging equipment.

Translational Relevance: AMDX-9101 detection of TTR amyloid may provide a potential new and noninvasive test for ATTR that could lead to earlier ATTR diagnosis, as well as facilitate development of new therapeutics.

Introduction

Transthyretin amyloidosis (ATTR) is among the most prevalent forms of systemic amyloidosis, a spectrum of diseases in which the deposition of amyloidogenic proteins and their amyloid fibrils in various tissues—including the heart, peripheral nerves, brain, gastrointestinal tract, kidneys, muscles, and eyes—leads to progressive organ toxicity and, in many forms of the disease, mortality.[1–8] More than 30 proteins are implicated as causes of amyloidosis, with more than 17 leading to multiorgan systemic pathology.[2,9] In the case of ATTR, the disease is caused by amyloidogenic deposition of the protein transthyretin (TTR), a transporter for both thyroxin and retinol that is synthesized mainly (80%) in the liver and also by choroid plexus, retinal pigment epithelium and

pancreatic α-cells.[8,10–13] There are two main types of ATTR[3,7,8,14,15]: (i) a hereditary form caused by >130 missense mutations in the *TTR* gene (variant TTR, or vATTR) and (ii) an age-related, male-predominant form linked to misfolding of the wild-type protein (wtATTR), previously known as *senile systemic amyloidosis*.[16] vATTR is a rare condition that is endemic to Portugal, Japan, Brazil, and Sweden[5,14,15,17–19] and is found at a low frequency in all populations, whereas wtATTR has a much higher estimated global prevalence of ~1/5800[20–22] and is thought to be greatly underdiagnosed.[21] In each form, whether through destabilizing mutations of *TTR* in vATTR or age-related changes in proteostasis in wtATTR, TTR protein dislodges from a homotetramer and misfolds, ultimately forming toxic deposits of native protein and amyloid fibrils in the extracellular milieu of various organs and tissues.[3,10,23]

Although TTR amyloid can infiltrate diverse tissues, the most common clinical manifestations of ATTR result from its deposition in heart and peripheral nerves, resulting in ATTR cardiomyopathy (ATTR-CM) and familial amyloid polyneuropathy (FAP), respectively. Both vATTR and, to a larger extent, wtATTR are significant causes of amyloid cardiomyopathy and peripheral neuropathy.[7,17,24,25] ATTR-CM can progress in an insidious manner with long periods of functional stability that invariably yield to severe heart failure. Median survival in wtATTR-CM patients is 3.5 years from diagnosis, with most cases occurring after age 60 (mean age = 80). In vATTR-CM patients, disease penetrance and clinical course vary by genotype and population.[7,26,27] The autosomal dominant V122I mutation in particular, which is present in 3% to 4% of African Americans with an onset between 67 to 71 years of age, is a major cause of vATTR-CM and carries the worst prognosis with a median survival after diagnosis of 2.5 years.[25,28–30] FAP can present with loss of superficial sensation, paresthesias, autonomic dysfunction, weakness, cardiac conduction abnormalities, and cachexia in its end stages. FAP is the prototypical disease caused by the most common ATTR mutation worldwide, the V30M substitution.[1,3,6,14,15] Signs of neuropathy in FAP can begin in the second decade of life, but frank symptoms typically manifest in the 30s to 50s.[14]

In addition to ATTR-CM and FAP, and often as co-presenting features, TTR can cause morbidity by depositing in other tissues. The central nervous system can be impacted by leptomeningeal deposition of vTTR amyloid locally synthesized by choroid plexus, leading to an array of symptoms including cognitive decline, seizures, hydrocephalus, and sensory and motor disturbances.[31] Notably, many ATTR patients exhibit ocular involvement in which TTR amyloid can accumulate in various parts of the eye, including the cornea, lens, iris, retinal pigment epithelium, ciliary pigment epithelium, vitreous, conjunctiva, trabecular meshwork, lacrimal glands, and retina.[32–34]

The treatment of ATTR has been transformed recently by the approval of several disease-modifying therapies.[3,27,30,35–39] Tafamidis (Vyndaqel and Vyndamax; Pfizer, New York, NY, USA) is a small molecule that binds to the T4 binding pocket of TTR and stabilizes the homotetramer, thus attenuating the first step in the cascade of events leading to amyloidogenesis. Available since 2011 in the EU for vATTR-FAP, Tafamidis is now approved in the United States for vATTR and wtATTR-CM. In addition, a trio of oligonucleotide (RNA) biologics have been approved for vATTR-FAP: Patisiran (Onpattro; Alnylam Pharmaceuticals, Cambridge, MA, USA), Inotersen (Tegsedi; Ionis Pharmaceuticals, Carlsbad, CA, USA), and Vutrisiran (Amvuttra, Alnylam Pharmaceuticals). These anti-sense and small interfering RNA therapies inhibit synthesis of TTR by targeting mRNAs encoding both mutant and wildtype proteins. These treatments, which may soon be complemented by a diverse set of therapeutics currently in the pipeline,[36] slow, stabilize, and in some settings improve outcomes. Importantly, they will provide more options and greater access to treatment than was possible with orthotopic liver transplantation (the only prior disease-modifying treatment) and transplantation of affected organs such as the heart. As has become axiomatic in the treatment of progressive diseases, earlier intervention with new ATTR therapeutics leads to better outcomes in both ATTR-CM and FAP.[36]

Current methods to diagnose ATTR include scintigraphy with bone-avid tracers, positron emission tomography imaging with amyloid tracers, and magnetic resonance imaging. Ironically, the broad benefits that can be achieved with new ATTR therapies in terms of quality of life and the high healthcare costs associated with advanced organ disease are at present restricted by marked inadequacies in the diagnosis of ATTR.[40–45] These methods are expensive and not widely available outside of major cities.

The accumulation of TTR amyloid in ocular and periocular tissues may provide a basis for noninvasive diagnosis of ATTR by way of a simple eye exam, provided that TTR amyloid can be labeled and imaged. Of particular interest in this regard is a report that demonstrated TTR amyloid in the conjunctiva in ~90% of FAP patients harboring the V30M mutation.[34] Conjunctival TTR deposits may

thus be a common feature of ATTR that reflects systemic disease, one that potentially can be exploited to enable a sensitive and early diagnosis of systemic ATTR. We report here a series of studies aimed at establishing early proof of concept that TTR amyloid in the conjunctiva can be fluorescently labeled with a novel compound, AMDX-9101, for detection with a standard ocular imaging system. AMDX-9101 is a member of a class of fluorescent, synthetic small molecule "ocular" tracers that bind β-sheet-rich amyloid and amyloid-like protein deposits and, upon binding, undergo a large ($\geq$10$\times$) increase in fluorescence quantum yield.

Material and Methods

The Wills Eye Hospital Institutional Review Board approved this retrospective study (IRB no. 2022-25) and deemed that informed consent was not required for this study. The study was performed in compliance with HIPAA guidelines and with the tenets of Declaration of Helsinki.

Patients and Tissue Selection

Wills Eye Hospital Department of Pathology records were searched for all representative cases of ocular ATTR amyloidosis with sufficient tissue for ancillary studies from the patients who met the clinical and genetic criteria for ATTR amyloidosis. Enucleated eyes, autopsy eyes, and conjunctival biopsy specimens with no or minimal pathology from patients with no history of amyloidosis were selected as controls. Data collected included patient age, sex, specimen type, and diagnosis.

Histopathology

Routine sections stained with hematoxylin-eosin and Congo red stains with appropriate controls were prepared from formalin-fixed paraffin-embedded (FFPE) tissues.

Immunostaining

FFPE sections 5 µm thick from ATTR amyloidosis and control eye samples were deparaffinized by immersion for five minutes in each of the following solutions: two times in 100% xylene, one time in 50% xylene/50% ethanol, and then three minutes in each of the following: 100% ethanol, 95% ethanol, 70% ethanol, and 50% ethanol and two times in water. For antigen retrieval, sections were treated with 99% formic acid for five minutes followed by three washes in water. Sections were boiled for 20 minutes in 0.01 M citrate buffer, pH of 6.0 (unmasking solution - H-3300; Vector Laboratories, Burlingame, CA, USA). Slides were cooled in water three times for five minutes followed by immersion in phosphate-buffered saline solution (PBS) for 15 minutes. Sections were blocked for one hour (5% normal goat serum and 0.1% Triton X-100 in PBS) at room temperature. Sections were incubated overnight at 4°C with the TTR primary antibody (Agilent no. A000202-2, 1:250). Tissues were washed three times with PBST for 10 minutes followed by the goat anti-Rabbit secondary antibody Alexa Fluor 647 (1:500; ThermoFisher, St. Louis, MO, USA) for one hour at room temperature. Sections were washed three times for 10 minutes in PBST and then stained with compound (60 µM) diluted in PBS for 30 minutes at room temperature. After three washes in PBS, tissues were incubated with 2 µg/mL Hoechst for 10 minutes. Sections were washed three times for 10 minutes in PBS and mounted with media (Prolong; Molecular Probes, Eugene, OR, USA).

Ex Vivo Human Cadaver Eye Image Acquisition and Analysis

Tissues stained with Congo red histochemical stain were examined in bright and polarized light using a Leica microscope (TM-ADD Model; Leica Microcystems, Wetzlar, Germany) equipped with a polarizer and analyzer. The characteristic green birefringent polarization color was taken as a proof of the presence of amyloid in the tissue. Fluorescent images were captured (20x/0.8 NA objective) by an Axio ScanZ1 scanner microscope (Carl Zeiss, Oberkochen, Germany) with ZEN2.3 slidescan module software using high-efficiency fluorescent filter sets for Hoechst, AF488/GFP, AF568, and AF647, which use 385, 475, 555, and 630 nm excitation. For high-resolution confocal microscopy, images were acquired on an inverted Zeiss LSM 780 (63 $\times$ 1.4 NA objective) using the ZEN blue software. To collect birefringence images, sections stained with Congo Red were illuminated under a polarizing filter attached to a Zeiss LSM780 microscope. Images were taken through the ocular lens to capture the apple-green birefringence effect, as well as through the LSM780 in the transmitted light channel. Congo red fluorescence accompanied by green birefringence was interpreted as a proof of the presence of amyloid in the tissue. Congo red fluorescence without green birefringence was interpreted as nonspecific fluorescence. Images were visualized and processed with ZEN lite and FIJI.

Measurement of Signal Intensity and TTR:AMDX-9101 Co-Localization

Regions from the TTR images were selected from four separate microscopic fields, which were adequately separated from each other and contained relatively higher TTR loads. All the images were analyzed by MATLAB R2022b version 9.13.0.2080170 (MathWorks, Inc., Natick, MA, USA) as follows; (1) Images were segmented based on pixel intensity to identify the foreground and background areas. Very bright (hot) pixels were excluded from the analysis. (2) Bright areas belonging to protein aggregates were selected as the foreground. (3) Dim cellular fluorescence pixels resulting from nonspecific labeling were selected as the background. (4) Pixels outside the cellular areas, whose intensity represents camera noise (dark and shot noise), were excluded from the analysis. Specifically, each image's foreground and background areas were identified by visual inspection for both control (n = 4) and TTR (n = 4) image datasets. The fluorescent signal-to-noise ratio was calculated as the average of the foreground pixels over the average of the background pixels. Results were plotted as box plots, indicating the twenty-fifth percentile (bottom boundary), median (middle line), seventy-fifth percentile (top boundary), and nearest observations within 1.5 times the interquartile range (whiskers). Co-localization between TTR and AMDX-9101 was quantified by using the ZEN module (Carl Zeiss). From conjunctival images, four specific regions of interest were delineated, and established minimum intensity thresholds were applied. Two fluorescent channels were chosen sequentially, and the software automatically calculated spatial overlap coefficients of pixel intensities between them using Mander's coefficient.

Aggregation of TTR

TTR aggregates were prepared as described by Frangolho et al.[46] Lyophilized TTR (Novus Biologicals NBP2-62523) was resuspended in 50 mM glycine buffer as a 100 µM stock. The solution was incubated at room temperature for 24 hours, and aliquots were kept at −80°C.

Binding Characterization of Compound With TTR

The binding of AMDX with TTR was characterized by measuring the fluorescent spectra. AMDX compound solution 4 µM was prepared with and without 5 µM of aggregated TTR in triplicates. The maximum absorbance, emission, and excitation wavelength of AMDX-9101 with and without aggregated TTR was measured on a Shimadzu RF-5301PC spectrophotometer with the LabSolutions RF software (Shimadzu, Kyoto, Japan). The fold increase was calculated by measuring the relative fluorescent unit of AMDX + TTR/AMDX. The binding affinity (Kd) of AMDX-9101 and TTR was obtained by measuring the emission of increasing AMDX-9101 (0–10 µM) with a constant TTR concentration (5 µM) using the previously measured maximum excitation of 440 nm. The Kd was determined by plotting the relative fluorescent unit at maximum emission (λmax em) with TTR versus probe concentration.

In Vitro and Ex Vivo Porcine Eye TTR:AMDX-9101 Binding Protocols

Nitrocellulose member discs (NMDs; 6 mm diameter; 28.26 mm^2) were cut using a hole puncher from nitrocellulose membranes (Thermo; 77012). NMDs were placed in 96-well dishes and incubated with 100 µL of TTR-aggregate protein (1.38 mg/mL) in PBS or PBS-alone for 30 minutes and air-dried for one hour. The NMDs were moved to separate 96-well plates and incubated with AMDX-9101 (100 µL; 15 µM) at RT for 30 minutes in the dark. The NMDs were then moved into six-well plates filled with 3 mL of PBS in each well, wrapped with aluminum foil, and placed on a shaker for three times PBS washes at 15 minutes each. To assess protein binding, Ponceau-S stain (P7170; Sigma-Aldrich Corp., St. Louis, MO, USA) was performed by soaking the NMDs in Ponceau-S solution for 30 seconds followed by a five-second water rinse. NMDs were air dried and then imaged using a digital camera. For in vitro fluorescence assessment, NMDs were imaged using a Spectralis HRA + OCT (Heidelberg Engineering, GmbH, Heidelberg, Germany) on a FLEX module. The Spectralis HRA+OCT is a camera that is routinely used in clinical care and potentially suitable for TTR detection using AMDX-9101 in a clinical setting. The camera head was placed above the NMDs, and images were centered in the frame using a 55° lens (~25 diopter scan focus). Fluorescence images were obtained, similar to previous report in ex vivo and human patient eyes,[47,48] using the fluorescein capture mode (excitation wavelength: 486 nm and transmission filter set at >500 nm) at a fixed sensitivity of 80 with image averaging set to 100 frames. For ex vivo eye assesement, porcine eyes were chosen because standard human enucleation technique involves removal of the eye without the conjunctiva. The conjunctiva is left with the donor and is closed to cover the orbital

cavity or an orbital implant. Thus, to have adequate conjunctiva, porcine eyes (n = 7; Yorkshire Cross-breed pigs) were acquired from an abattoir (Sierra for Medical Science, Inc., Whitter, CA, USA) and shipped on blue ice within 24 hours of death. Excess tissue was trimmed upon arrival. The subconjunctival space was dissected free from the underlying sclera using small Westcott scissors and forceps. NMDs were grasped and placed under the porcine conjunctiva in an area with sufficient conjunctival skirt to fully cover the NMD. Fluorescence imaging was performed as above for the in vitro studies except that the sensitivity setting was set at 107 for all cases to capture fluorescence signal through the porcine conjunctival tissue. For image analyses, acquired images were opened using Image J (NIH, Bethesda, MD, USA). A circular region of interest (ROI; 19.6 mm^2 diameter) was established. Using this ROI, fluorescence intensity was measured from the surface of the eye on the NMD and on the surface of the eye away from the NMD to collect background signal. The relative fluorescence intensity was calculated by dividing the fluorescence on the NMD over that of the background region. In this case, and as an example, a value of 1 would indicate that the queried ROI has fluorescence intensity equivalent to background.

Results

In vitro Evaluation of AMDX-9101 as a Fluorescent Tracer for TTR Amyloid

AMDX-9101 belongs to a novel class of amyloid-binding synthetic small molecule fluorophores that are being developed to label and visualize disease-related biomarkers in the eye.[49] The suitability of AMDX-9101 as a hyperfluorescent tracer for TTR amyloid was evaluated first in vitro. Human wtTTR was aggregated in vitro into thioflavin T-positive aggregates according to published protocols.[46,50] The absorbance, emission, and excitation profiles of AMDX-9101 were then measured in reactions containing 4 µM of AMDX-9101 in solution with and without 5 µM of TTR aggregates, and the fold increase in fluorescence induced by TTR was calculated. The peak fluorescence emission of AMDX-9101 (549 nm) was enhanced approximately 27-fold upon incubation with aggregated TTR, compared to fluorescence in the absence of TTR, while excited at 450 nm (Fig. 1A). The binding of AMDX-9101 to aggregated TTR was characterized over a concentration range of 0 to 10 µM tracer with a constant 5 µM of TTR aggregates. AMDX-9101 bound to aggregated TTR in solution with an appar-

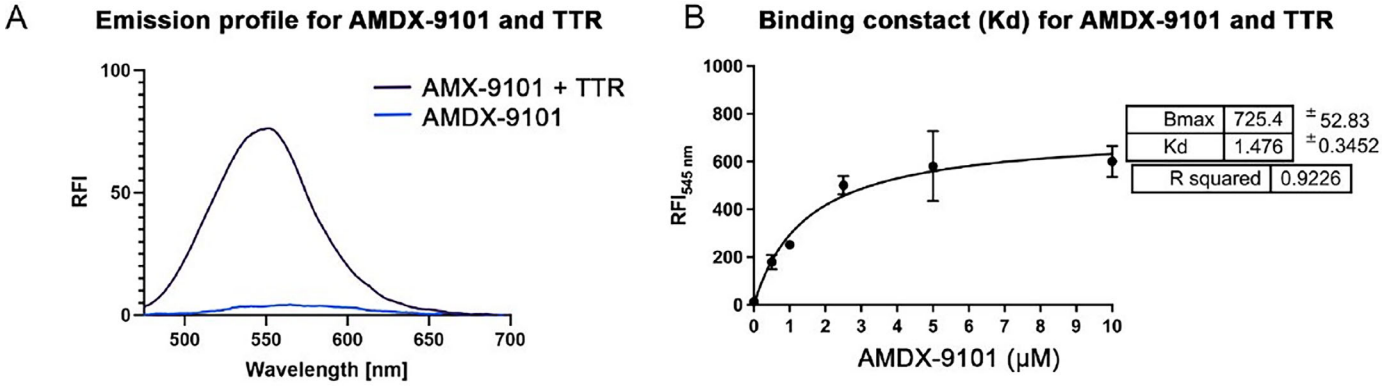

C

Compound	λmax Excitation Bound (nm)	λmax Emission Bound (nm)	K_d (µM)	Fold Increase
AMDX-9101	467	549	1.476 ± 0.3452	27.6

Figure 1. Spectroscopic and binding properties of AMDX-9101 combined with aggregated wild type TTR. (**A**) Fluorescent emission of AMDX-9101 before (*blue*) and after (*purple*) mixing with TTR aggregates. (**B**) Plot of the fluorescence intensity (λ_{max} = 545 nm) as a function of the concentration of AMDX-9101 in the presence of aggregated TTR peptides (5 µM) in solution. Fitting this data to the equation: y = Bx/(Kd + x) revealed a Kd of 1.476 ± 0.3452 µM for association of AMDX-9101 to aggregated TTR peptides. (**C**) Spectroscopic properties of AMDX-9101 and wt TTR. Fold increase determined from the emission with 4 µM AMDX and 5 µM aggregated TTR at the maximum emission of AMDX + TTR.

ent dissociation constant (Kd) of 1.476 ± 0.3452 µM (Fig. 1B). The maximum wavelengths for excitation and emission of TTR-bound AMDX-9101 were determined and were within ranges used by ophthalmic imaging devices that are used widely in eye care clinics (λ_{ex} 467 nm, λ_{em} 549 nm; Fig. 1C). These in vitro results indicated that AMDX-9101 binds to TTR amyloid and hyperfluoresces and that its spectral properties are well suited for use as an in vivo TTR amyloid fluorescent ocular contrast agent.

AMDX-9101 Labeling of TTR in Ex Vivo Human Ocular Tissue From ATTR Amyloidosis Patients

We next evaluated whether AMDX-9101 could enable visualization of TTR amyloid in human ocular samples of ATTR amyloidosis. To obtain tissues for the study, representative cases of ocular ATTR amyloidosis in patients who were seen at the Wills Eye Hospital and met the clinical and genetic criteria for ATTR amyloidosis were reviewed. The pathology records revealed two patients with clinically and genetically documented ATTR amyloidosis with sufficient tissue available for additional studies. One patient underwent enucleation for a blind and painful eye with end-stage primary open angle glaucoma (87-year-old female with FAP type II TTR mutation [serine 84] TTR amyloidosis), and the second patient underwent pars plana vitrectomy with vitreous biopsy (77-year-old male with hATTR mutation [TTR c.148G>A; p.Val50Met heterozygous missense, autosomal dominant]). Two previously untreated enucleated eyes in adult patients with uveal melanoma, one autopsy eye with no appreciable pathology from an infant, and five conjunctival biopsy specimens with no appreciable pathology were selected as controls. Patient characteristics and pathological diagnoses are summarized in the Table.

To confirm the presence (or absence in the case of controls) of TTR amyloid, FFPE tissues were stained with hematoxylin-eosin and Congo red histochemical and fluorescent stains. Tissues stained with Congo red were examined in bright and polarized light for characteristic green birefringent polarization color as a proof of the presence of amyloid in the tissue (Fig. 2, left column). Serially adjoining FFPE cross-sections from the same area were then analyzed by immunofluorescence with an antibody to TTR, and counterstained with AMDX-9101. In the enucleated eye with ATTR amyloidosis, there was colocalization of high signal intensity AMDX-9101 fluorescence and TTR immunofluorescence (Fig. 2, right column, yellow). Congo red-positive regions that were also labeled by AMDX-9101 and TTR antibody were detected in the episcleral vessels, orbital posterior ciliary arteries and nerves, sclera (most prominent adjacent to emissarial canals and episcleral vessels), inner retina, vitreous, and optic nerve sheath (Table, Fig. 2). AMDX-9101 and TTR showed strong signal colocalization in the conjunctival vessels, whereas corresponding Congo red histochemical and fluorescence preparations were negative, suggesting that AMDX-9101 and TTR immunofluorescence labeling are more sensitive in detection of TTR amyloid in the conjunctiva when compared to traditional Congo red staining methods. We observed a high-intensity AMDX-9101 signal in the conjunctival and corneal epithelia, whereas Congo red-green birefringence and TTR stains were negative; this finding was not seen in controls. Using conjunctival tissue, we quantitated the level of colocalization between TTR and AMDX-9101. Overall, 86.9% ± 1.4% of AMDX-9109 signal colocalized with immunostained TTR in the TTR amyloidosis sample, whereas no colocalization was observed in the control ($P < 0.001$). Of note, we did not see amyloid deposition in the anterior chamber angle or corneal stroma with any of our methods in the enucleated ATTR eye. A vitrectomy sample from a patient with ATTR amyloidosis demonstrated findings similar to the vitreous in the enucleated eye.

There was no evidence of amyloid deposits by Congo red histochemical and fluorescence methods, TTR amyloid deposits, or strong AMDX-9101 signal in any of the control samples (Fig. 3). We noted weak intensity AMDX-9101 signal in the uvea, retina, sclera, optic nerve sheath, orbital vessels/nerves, orbital extraocular muscle, and conjunctiva (diffuse weak fluorescence). AMDX-9101 faintly stained background collagen, muscle, and nerves in tissues of patients with ATTR and in control tissues. Corresponding Congo red fluorescent preparations demonstrated weak red fluorescence but did not show green birefringence, and TTR fluorescence stains were all negative in these tissues; thus the findings were interpreted as nonspecific staining.

To quantify the fluorescent signal intensity of TTR-bound AMDX-9101, regions from the ex vivo stained tissues were selected from four separate microscopic fields that contained relatively higher TTR loads as assessed by immunofluorescence for TTR. Images taken from the FAP type II TTR mutation patient in the optic nerve, posterior ciliary arteries and nerves, and the conjunctiva were compared to controls in the same regions. The fluorescent signal-to-noise ratio was calculated as the average of the foreground

Table. Transthyretin Amyloidosis and Controls: Patient and Biopsy Characteristics and Study Results

Patient Age, Sex	Diagnosis	Specimen Type	Tissue Evaluated	Study Results				
				Congo Red (H)	Congo Red (F)–Green	AMDX-9101	TTR	AMDX-9101 + TTR Co-Staining
87 F	ATTR *TTR* c.311T>G (p.Ile104Ser)	Eyeball	Conjunctiva	Negative	Negative	Positive (strong)	Positive (strong)	Positive (strong)
			Cornea					
			Sclera	Positive	Positive	Positive (strong)	Positive (strong)	Positive (strong)
			Uvea	Negative*	Negative	Negative	Negative	Negative
			Vitreous	Positive	Positive	Positive (strong)	Positive (strong)	Positive (strong)
			Retina	Negative	Negative	Positive (strong)	Positive (strong)	Positive (strong)
			Optic nerve (sheath)	Positive	Positive	Positive (strong)	Positive (strong)	Positive (strong)
			Orbit	Positive	Positive	Positive (strong)	Positive (strong)	Positive (strong)
77 M	ATTR *TTR* c.148G>A (p.val50Met)	Vitreous		Positive	Positive	Positive (strong)	Positive (strong)	Positive (strong)
74 M	Control - uveal melanoma	Eyeball	Conjunctiva	N/A	N/A	N/A	N/A	N/A
			Cornea	Negative	Negative	Negative	Negative	Negative
			Sclera	Negative	Negative	Positive (weak)	Negative	Negative
			Uvea	Negative	Negative	Negative	Negative	Negative
			Vitreous	Negative	Negative	Negative	Negative	Negative
			Retina	Negative	Negative	Positive (weak)	Negative	Negative
			Optic nerve	Negative	Negative	Positive (weak)	Negative	Negative
			Orbit	Negative	Negative	Positive (weak)	Negative	Negative
62 M	Control - uveal melanoma	Eyeball	Conjunctiva	N/A	N/A	N/A	N/A	N/A
			Cornea	Negative	Negative	Negative	Negative	Negative
			Sclera	Negative	Negative	Positive (weak)	Negative	Negative
			Uvea	Negative	Negative	Positive (weak)	Negative	Negative
			Vitreous	Negative	Negative	Negative	Negative	Negative
			Retina	Negative	Negative	Negative	Negative	Negative
			Optic nerve	Negative	Negative	Positive (weak)	Negative	Negative
			Orbit	Negative	Negative	Positive (weak)	Negative	Negative
3 M	Control - autopsy	Eyeball	Conjunctiva	Negative	Negative	Positive (weak)	Negative	Negative
			Cornea	Negative	Negative	Negative	Negative	Negative
			Sclera	Negative	Negative	Positive (weak)	Negative	Negative
			Uvea	Negative	Negative	Negative	Negative	Negative
			Vitreous	Negative	Negative	Negative	Negative	Negative
			Retina	Negative	Negative	Positive (weak)	Negative	Negative
			Optic nerve	Negative	Negative	Positive (weak)	Negative	Negative
			Orbit	Negative	Negative	Positive (weak)	Negative	Negative
57 M	Control - conjunctival melanosis without atypia	Conjunctiva		Negative	Negative	Negative	Negative	Negative
76 F	Control - conjunctival melanosis without atypia	Conjunctiva		Negative	Negative	Negative	Negative	Negative
83 M	Control - normal mapping biopsy for sebaceous carcinoma	Conjunctiva		Negative	Negative	Positive (weak)	Negative	Negative
79 F	Control - normal mapping biopsy for sebaceous carcinoma	Conjunctiva		Negative	Negative	Positive (weak)	Negative	Negative
79 F	Control - normal mapping biopsy for sebaceous carcinoma	Conjunctiva		Negative	Negative	Positive (weak)	Negative	Negative

ATTR, transthyretin amyloidosis; F, female; F, fluorescent stain; H, histochemical stain; M, male; TTR, transthyretin.

*Original sections had Congo red-positive material around choroidal vessels—this was absent in recut sections.

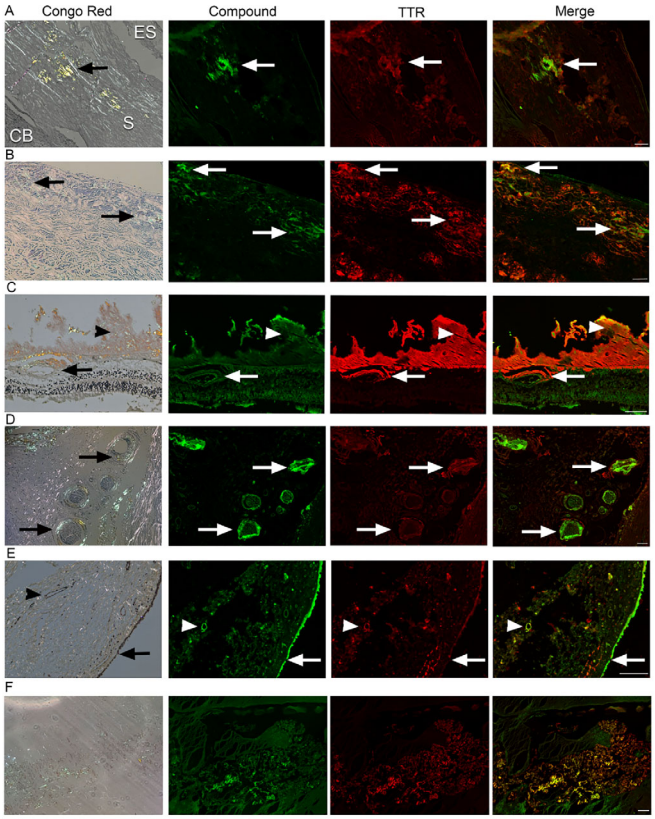

Figure 2. Ex vivo co-staining of AMDX-9101 and TTR in human ATTR amyloidosis eye. FFPE ocular sections from a human ATTR amyloidosis eye were either (**1**) stained with Congo red and examined in bright and polarized light using a Leica microscope equipped with a polarizer and analyzer. The characteristic green birefringent polarization color was taken as proof of the presence of amyloid in the tissue (*left column*) or (**2**) FFPE sections were co-stained with AMDX-9101 (*green*) and TTR antibody (*red*). Overlay of all channels shows colocalization in *yellow*. *Scale bar* = 100 µm. Images taken from 87-year-old man with FAP type II TTR mutation (serine 84) TTR amyloidosis: (**A**) Sclera adjacent to emissarial canals (ES, episclera; S, sclera; CB, ciliary body; *arrows*, amyloid); (**B**) Optic nerve sheath (*arrows*, amyloid); (**C**) Retina and vitreous, amyloid deposits around retinal vessels (*arrows*) and in the vitreous (*arrowhead*); (**D**) Posterior ciliary arteries and nerves (*arrows*); (**E**) Conjunctiva, epithelium (*arrows*), and vessels in the stroma (*arrowheads*). (**F**) Vitreous amyloid from an hATTR patient (TTR c.148G>A; p.Val50Met heterozygous missense, autosomal dominant).

pixels over the average of the background pixels. Results were plotted as box plots (Fig. 4), indicating the 25th percentile (bottom boundary), median (middle line), 75th percentile (top boundary), and nearest observations within 1.5-times the interquartile range (whiskers). The average signal-to-noise ratio of AMDX-9101-labeled TTR deposits was approximately 6, which was threefold higher than the signal in control samples (TTR: 6.08 ± 0.2 vs. control: 2.2 ± 0.29; $P < 0.001$) (Fig. 4).

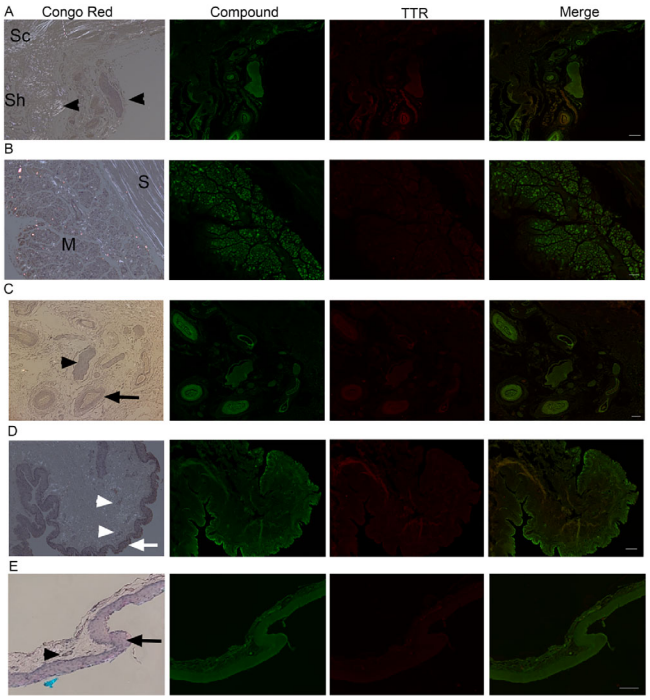

Figure 3. Ex vivo ocular images in human controls. FFPE ocular sections from human control eyes were either stained with Congo red and examined in bright and polarized light using a Leica microscope equipped with a polarizer and analyzer (the characteristic green birefringent polarization color was taken as a proof of the presence of amyloid in the tissue, left column) or co-stained with AMDX-9101 (*green*) and the TTR antibody (*red*). Overlay of all channels shows absence of colocalization in yellow. *Scale bar* = 100 µm. (**A**–**C**) From a 62-year-old patient with uveal melanoma: (**A**) optic nerve sheath (Sh), sclera (Sc), and posterior ciliary arteries/nerves (*arrowheads*). Note intrinsic yellow-white birefringence of the collagen, (**B**) sclera (S), and extraocular muscles (M), and (**C**) posterior ciliary arteries (*arrow*) and nerves (*arrowhead*). (**D**) Conjunctiva from three-year-old patient, epithelium (*arrow*), vessels in the stroma (*arrowheads*). (**E**) Conjunctiva from healthy adult, epithelium (*arrow*), vessel (*arrowheads*).

Visualization of TTR in the Conjunctiva Using AMDX-9101 in an Ex Vivo Porcine Eye Model

Based on the results from our histological studies, we next sought to determine whether AMDX-9101 could be used to visualize TTR deposits (wild type) in the conjunctiva. To this end, we created an ex vivo porcine eye model in which TTR aggregates were surgically implanted under postmortem porcine conjunctiva. Nitrocellulose membrane discs (NMDs) were cut and incubated with TTR aggregates that were dissolved in PBS. A PBS-alone condition served as a control. All NMDs were also incubated with AMDX-9101 (15 µM). Ponceau-S staining demonstrated successful binding of TTR protein to the NMDs (Fig. 5A), as evidenced by red Ponceau-S

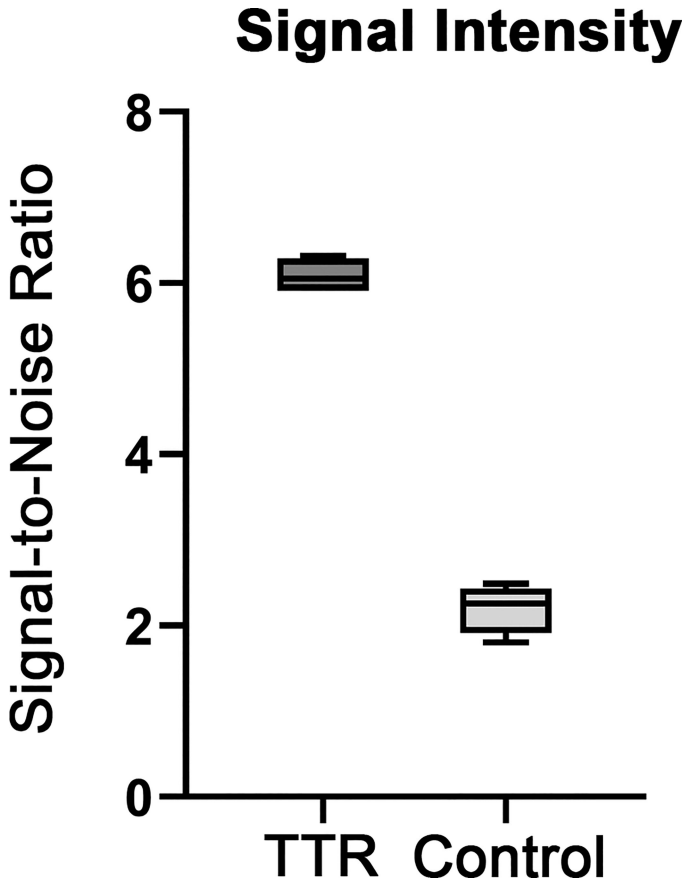

Figure 4. Quantification of AMDX-9101 signal intensity. Regions were selected from four separate fields. All images were analyzed by MATLAB R2022b. The fluorescent signal-to-noise ratio was calculated as the average of the foreground pixels over the average of the background pixels. Results were plotted as box plots, indicating the twenty-fifth percentile (*bottom boundary*), median (*middle line*), seventy-fifth percentile (*top boundary*), and nearest observations within 1.5 times the interquartile range (*whiskers*).

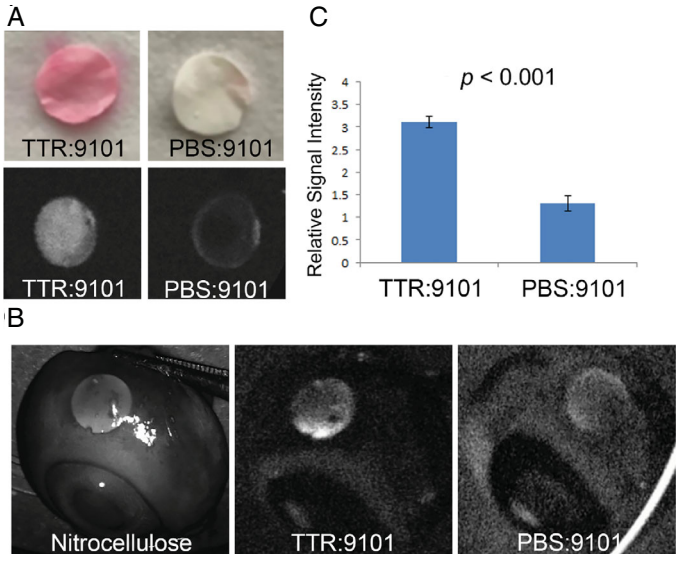

Figure 5. Visualization of TTR with AMDX-9101 in an ex vivo porcine eye model. (**A**) Nitrocellulose membrane discs (NMDs) were cut and incubated with TTR protein and AMDX-9101 and stained with Ponceau-S (*top panel*). Fluorescence images were taken using a Spectralis angiographic camera, demonstrating fluorescence with AMDX-9101. (**B**) TTR:AMDX-9101 NMDs (n = 4) and PBS:AMDX-9101 NMDs (n = 3) were placed under porcine conjunctiva for visualization using the Spectralis angiographic camera. (**C**) The relative fluorescence signal intensity of the subconjunctival NMDs were quantified in Image J from fluorescent images taken using the Spectralis camera.

stain. No red Ponceau-S stain was seen in the PBS-alone condition (Fig. 5A). Fluorescence imaging using a readily accessible ophthalmic camera (Spectralis HRA+OCT; Heidelberg Engineering, GmbH) also demonstrated fluorescence and specific binding of AMDX-9101 to the NMD-bound TTR aggregates (Fig. 5A). This was not seen in the PBS-alone NMDs (Fig. 5A). To evaluate whether AMDX-9101-labeled TTR aggregates could be detected under the conjunctiva, postmortem ex vivo pig eyes were acquired, and the subconjunctival space was dissected free from the underlying sclera. Then TTR:AMDX-9101 NMDs (n = 4) or PBS:AMDX-9101 NMDs (n = 3) were placed under the conjunctiva for testing. Fluorescence images were collected using the Spectralis HRA + OCT ophthalmic device to demonstrate fluorescence and specific binding of AMDX-9101 to the TTR-bound NMDs (Fig. 5B). Fluorescent signal above background was observed through porcine conjunctiva for the TTR: AMDX-9101 NMDs (Fig. 5B). However, no fluorescent signal above background fluorescence was observed through porcine conjunctiva for PBS: AMDX-9101 NMDs (Fig. 5B). The fluorescence of the subconjunctival complex NMDs was quantified, revealing a nearly 3-fold increase in fluorescence imaged from the TTR:AMDX-9101 NMDs compared to the PBS:AMDX-9101 NMDs (3.10 ± 0.13 [TTR:AMDX-9101] vs. 1.30 ± 0.17 [PBS:AMDX-9101]; $P < 0.001$) (Fig. 5C).

Discussion

In this study, we demonstrated that AMDX-9101—an amyloid binding fluorescent ocular tracer—hyperfluoresces upon binding to TTR amyloid in vitro, labels TTR amyloid in conjunctiva and other ocular tissues from patients with vATTR and supports detection of TTR amyloid using a readily accessible and widely used ophthalmic imaging device in an ex vivo porcine model of conjunctival TTR amyloid deposition. In vitro, peak fluorescence emission of AMDX-9101 was increased 27-fold by addition of aggregated TTR,

suggesting that the tracer can generate a high signal-to-noise label of TTR amyloid in situ. Accordingly, AMDX-9101 marked areas that were immunopositive for TTR deposition in conjunctiva and ocular tissues from vATTR patients with a signal-to-noise ratio of approximately 6, which is threefold higher than the signals observed in control specimens. Moreover, this signal in vATTR specimens was deemed superior to that generated by Congo red staining in adjacent serial sections. In the porcine eye model, fluorescence emission from AMDX-9101-labeled TTR aggregates that were implanted into the conjunctiva on a nitrocellulose matrix was sufficient to enable detection with an ophthalmic imaging device that is widely used in eye care practices. These data raise the possibility that AMDX-9101, when delivered to the eye as a topical formulation, could be used as the basis for a novel approach to diagnosing ATTR by way of a simple eye examination. This possibility takes on special significance considering the emergence of newly approved and existing disease-modifying treatments for ATTR and the consensus view that ATTR is greatly underdiagnosed,[40–45] particularly among older adults and African Americans who carry the V122I mutation.[25,29,51,52]

There is an emerging consensus that large diagnostic shortfalls for ATTR exist, stemming from a set of interacting factors that prevent, delay or confuse diagnosis, including the following: (i) lack of awareness among primary care physicians of ATTR or its early signs, (ii) heterogeneity of presentation, (iii) diverse symptoms that can be mimicked by more common conditions (particularly in the elderly with wtATTR), (iv) low sensitivity of first-pass diagnostic approaches, and (v) limited access to or ordering of specialized nuclear imaging tests.[40–45] Moreover, patients who do obtain a definitive diagnosis only receive one after a long and arduous medical journey[41] that delays therapeutic intervention. The mean diagnostic delay is 6.1 years for wtATTR-CM and 5.7 years for vATTR-CM,[40] during which 34% to 57% of patients will have previously received one or more non-ATTR-CM diagnoses and 25% will have seen five or more doctors.[40,42,43] Misdiagnosis remains a factor even when ATTR-CM patients are seen by a cardiologist—up to 13 different cardiac diagnoses are erroneously made, with hypertensive CM and hypertrophic CM being among the most frequent.[40] Remarkably, the probability of vATTR-CM patients receiving a cardiac magnetic resonance imaging or ^{99m}Tc-pyrophosphate scintigraphy—the latter having a very high specificity and sensitivity for ATTR-CM[25,53–57]—remains below 0.1 at five years.[40,41] Thus, although diagnostic imaging protocols can capture ATTR-CM with high precision, their application is low. Compounding the problem is that clinical suspicion of ATTR remains low as well,[40–45] particularly early on when most doctors do not catch early signs of the disease, such as carpal tunnel syndrome in the elderly (which can precede symptoms by five to 15 years) and lumbar stenosis.[58–61]

One of the most frequently used first-line tests for amyloidosis—fat pad biopsy with Congo Red staining—has a very low sensitivity for ATTR: <45% for vATTR and <15% for wtATTR.[62,63] The same challenges of diagnostic capture rate apply to FAP (as well as gastrointestinal and other manifestations of ATTR), where patients see multiple doctors and receive multiple misdiagnoses over a four-year or more period before getting a definitive diagnosis.[41,42]

Development of a new diagnostic for ATTR based on imaging of conjunctival TTR amyloid with topically applied AMDX-9101 could in principle overcome awareness, cost, and technical and accessibility barriers to capture more ATTR patients and do so at earlier stages of disease to maximize the quality-of-life and economic benefits of new therapeutics. The full potential of such an approach awaits further studies on whether TTR amyloid accumulates in the conjunctiva in the context of wt-ATTR and mutations other than the V30M substitution, and if it does so at presymptomatic stages of disease. Should this be the case, the elderly and African Americans carrying the V122I substitution stand to benefit most from improvements in ATTR diagnosis offered by an ocular approach because they are at greater risk for developing ATTR-CM and for receiving a delayed diagnosis, a misdiagnosis, or having their underlying ATTR disease go completely unrecognized. In African Americans the already-low use of definitive ATTR diagnostics and access to healthcare professionals that recognize symptoms of ATTR is compounded by demographic differences in healthcare access.[25,29,30,41,52]

Perhaps the most catalytic factor of an ocular approach to diagnosing ATTR is that it would shift the physician demographic tasked with recognizing and screening for ATTR to eye care professionals. In the United States, use of eye care is relatively high among older adults.[64,65] A recent survey found that approximately 82% of Americans between the ages 50 and 80—an age range that spans the presymptomatic to symptomatic phases of wtATTR-CM and V122I ATTR-CM—had an eye examination within the last two years.[64] Access to eye care professionals is also high for this age group; 90% of the Medicare population lives (USA) within 25 minutes of an ophthalmologist and 14 minutes of an optometrist.[66] Both ophthalmologists and optometrists use ocular imaging systems that can capture AMDX-9101 signals and can

perform external application of a topically formulated contrast agent to the conjunctiva. The rates and ease of eye care use make this physician demographic an excellent potential capture point for ATTR diagnosis and monitoring. Equipping ophthalmologists and optometrists with a simple, low cost, noninvasive test for conjunctival TTR amyloid could dramatically increase the scale of ATTR capture through routine or age- or demographic-triggered screening protocols.

In conclusion, this early preclinical study demonstrates the potential for AMDX-9101 to be used as an adjunctive diagnostic test for ATTR. Limitations of this study include the small sample size of available human tissue and the lack of samples from WT-ATTR cases. The use of postmortem animal eyes to test feasibility of imaging using clinically available ophthalmic imaging cameras is another limitation. Future studies will include studying AMDX-9101 ocular penetration, dose-finding, and eventual clinical study to establish safety and potential efficacy for AMDX-9101 to be used in patients with ATTR.

Acknowledgments

The authors thank the La Jolla Institute for Immunology microscopy and histology core for their assistance with image acquisition.

Disclosure: **J. Pilotte**, Amydis (E); **A.S. Huang**, Amydis (F); **S. Khoury**, Amydis (E); **X. Zhang**, None; **A. Tafreshi**, Amydis (C); **P. Vanderklish**, Amydis (E); **S.T. Sarraf**, Amydis (O); **J.S. Pulido**, Amydis (F); **T. Milman**, None

References

1. Andrade C. A peculiar form of peripheral neuropathy; familiar atypical generalized amyloidosis with special involvement of the peripheral nerves. *Brain.* 1952;75:408–427.
2. Muchtar E, Dispenzieri A, Magen H, et al. Systemic amyloidosis from A (AA) to T (ATTR): a review. *J Intern Med.* 2021;289:268–292.
3. Koike H, Katsuno M. Transthyretin amyloidosis: update on the clinical spectrum, pathogenesis, and disease-modifying therapies. *Neurol Ther.* 2020;9:317–333.
4. Cohen OC, Wechalekar AD. Systemic amyloidosis: moving into the spotlight. *Leukemia.* 2020;34:1215–1228.
5. Wechalekar AD, Gillmore JD, Hawkins PN. Systemic amyloidosis. *Lancet.* 2016;387(10038):2641–2654.
6. Plante-Bordeneuve V. Transthyretin familial amyloid polyneuropathy: an update. *J Neurol.* 2018;265:976–983.
7. Ruberg FL, Grogan M, Hanna M, Kelly JW, Maurer MS. Transthyretin Amyloid Cardiomyopathy: JACC State-of-the-Art Review. *J Am Coll Cardiol.* 2019;73:2872–2891.
8. Adams D, Koike H, Slama M, Coelho T. Hereditary transthyretin amyloidosis: a model of medical progress for a fatal disease. *Nat Rev Neurol.* 2019;15:387–404.
9. Benson MD, Buxbaum JN, Eisenberg DS, et al. Amyloid nomenclature 2018: recommendations by the International Society of Amyloidosis (ISA) nomenclature committee. *Amyloid.* 2018;25:215–219.
10. Sanguinetti C, Minniti M, Susini V, et al. The journey of human transthyretin: synthesis, structure stability, and catabolism. *Biomedicines.* 2022;10:1906.
11. Jacobsson B. Localization of transthyretin-mRNA and of immunoreactive transthyretin in the human fetus. *Virchows Arch A Pathol Anat Histopathol.* 1989;415:259–263.
12. Cavallaro T, Martone RL, Dwork AJ, Schon EA, Herbert J. The retinal pigment epithelium is the unique site of transthyretin synthesis in the rat eye. *Invest Ophthalmol Vis Sci.* 1990;31:497–501.
13. Su Y, Jono H, Misumi Y, et al. Novel function of transthyretin in pancreatic alpha cells. *FEBS Lett.* 2012;586:4215–4222.
14. Gertz MA. Hereditary ATTR amyloidosis: burden of illness and diagnostic challenges. *Am J Manag Care.* 2017;23(7 Suppl):S107–S112.
15. Adam MP, Mirzaa GM, Pagon RA, et al., eds. *GeneReviews*. Seattle: University of Washington, Seattle, 1993.
16. Pitkänen P, Westermark P, Cornwell GG, 3rd. Senile systemic amyloidosis. *Am J Pathol.* 1984;117:391–399.
17. Obi CA, Mostertz WC, Griffin JM, Judge DP. ATTR Epidemiology, genetics, and prognostic factors. *Methodist Debakey Cardiovasc J.* 2022;18(2):17–26.
18. Koike H, Misu K-I, Ikeda S-I, et al. Type I (Transthyretin Met30) familial amyloid polyneuropathy in Japan: early- vs late-onset form. *Arch Neurol.* 2002;59:1771–1776.
19. Misu K, Hattori N, Nagamatsu M, et al. Late-onset familial amyloid polyneuropathy type I (transthyretin Met30-associated familial amyloid

polyneuropathy) unrelated to endemic focus in Japan. Clinicopathological and genetic features. *Brain.* 1999;122(Pt 10):1951–162.
20. Palladini G. Wild type ATTR amyloidosis. Available at: https://www.orpha.net/consor/cgi-bin/OC_Exp.php?lng=EN&Expert=330001. Accessed January 08, 2023.
21. Porcari A, Fontana M, Gillmore JD. Transthyretin cardiac amyloidosis. *Cardiovasc Res.* 2023;118:3517–3535.
22. Antonopoulos AS, Panagiotopoulos I, Kouroutzoglou A, et al. Prevalence and clinical outcomes of transthyretin amyloidosis: a systematic review and meta-analysis. *Eur J Heart Fail.* 2022;24:1677–1696.
23. Koike H, Katsuno M. Ultrastructure in transthyretin amyloidosis: from pathophysiology to therapeutic insights. *Biomedicines.* 2019;7(1):11.
24. González-López E, Gallego-Delgado M, Guzzo-Merello G, et al. Wild-type transthyretin amyloidosis as a cause of heart failure with preserved ejection fraction. *Eur Heart J.* 2015;36:2585–2594.
25. Buxbaum JN, Ruberg FL. Transthyretin V122I (pV142I)* cardiac amyloidosis: an age-dependent autosomal dominant cardiomyopathy too common to be overlooked as a cause of significant heart disease in elderly African Americans. *Genet Med.* 2017;19:733–742.
26. Maurer MS, Hanna M, Grogan M, et al. Genotype and phenotype of transthyretin cardiac amyloidosis: THAOS (Transthyretin Amyloid Outcome Survey). *J Am Coll Cardiol.* 2016;68:161–172.
27. Irabor B, McMillan JM, Fine NM. Assessment and management of older patients with transthyretin amyloidosis cardiomyopathy: geriatric cardiology, frailty assessment and beyond. *Front Cardiovasc Med.* 2022;9:863179.
28. Jacobson DR, Alexander AA, Tagoe C, Buxbaum JN. Prevalence of the amyloidogenic transthyretin (TTR) V122I allele in 14 333 African-Americans. *Amyloid.* 2015;22:171–174.
29. Alexander KM, Falk RH. V122I TTR cardiac amyloidosis in patients of African descent: recognizing a missed disease or the dog that didn't bark? *Circ Heart Fail.* 2016;9(9):e003489.
30. Chandrashekar P, Alhuneafat L, Mannello M, et al. Prevalence and outcomes of p.Val142Ile TTR amyloidosis cardiomyopathy: a systematic review. *Circ Genom Precis Med.* 2021;14(5):e003356.
31. Qin Q, Wei C, Piao Y, et al. Current review of leptomeningeal amyloidosis associated with transthyretin mutations. *Neurologist.* 2021;26:189–195.
32. Beirão JM, Malheiro J, Lemos C, Beirão I, Costa P, Torres P. Ophthalmological manifestations in hereditary transthyretin (ATTR V30M) carriers: a review of 513 cases. *Amyloid.* 2015;22:117–122.
33. Dammacco R, Merlini G, Lisch W, et al. Amyloidosis and ocular involvement: an overview. *Semin Ophthalmol.* 2020;35:7–26.
34. Haraoka K, Ando Y, Ando E, et al. Amyloid deposition in ocular tissues of patients with familial amyloidotic polyneuropathy (FAP). *Amyloid.* 2002;9:183–189.
35. Ioannou A, Fontana M, Gillmore JD. RNA targeting and gene editing strategies for transthyretin amyloidosis. *BioDrugs.* 2023;37:127–142.
36. Tsoi MR, Lin JH, Patel AR. Emerging therapies for transthyretin amyloidosis. *Curr Oncol Rep.* 2023;25:549–558.
37. Gonzalez-Lopez E, Escobar-Lopez L, Obici L, et al. Prognosis of transthyretin cardiac amyloidosis without heart failure symptoms. *JACC CardioOncol.* 2022;4:442–454.
38. Cruz Rodriguez JB, Tallaj JA. Narrative review of pharmacotherapy for transthyretin cardiac amyloid. *Ann Transl Med.* 2021;9:519.
39. Park J, Egolum U, Parker S, Andrews E, Ombengi D, Ling H. Tafamidis: a first-in-class transthyretin stabilizer for transthyretin amyloid cardiomyopathy. *Ann Pharmacother.* 2020;54:470–477.
40. Rozenbaum MH, Large S, Bhambri R, et al. Impact of Delayed diagnosis and misdiagnosis for patients with transthyretin amyloid cardiomyopathy (ATTR-CM): a targeted literature review. *Cardiol Ther.* 2021;10:141–159.
41. Vera-Llonch M, Reddy SR, Chang E, Tarbox MH, Pollock M. The patient journey toward a diagnosis of hereditary transthyretin (ATTRv) amyloidosis. *Orphanet J Rare Dis.* 2021;16(1):25.
42. Gertz M, Adams D, Ando Y, et al. Avoiding misdiagnosis: expert consensus recommendations for the suspicion and diagnosis of transthyretin amyloidosis for the general practitioner. *BMC Fam Pract.* 2020;21:198.
43. Maurer MS, Bokhari S, Damy T, et al. Expert consensus recommendations for the suspicion and diagnosis of transthyretin cardiac amyloidosis. *Circ Heart Fail.* 2019;12(9):e006075.
44. Vergaro G, Solal AC, Emdin M. Wild type transthyretin amyloidosis: don't miss diagnosis! *Int J Cardiol.* 2020;312:96–97.
45. Galant NJ, Westermark P, Higaki JN, Chakrabartty A. Transthyretin amyloidosis: an under-recognized neuropathy and cardiomyopathy. *Clin Sci.* 2017;131:395–409.

46. Frangolho A, Correia BE, Vaz DC, Almeida ZL, Brito RMM. Oligomerization profile of human transthyretin variants with distinct amyloidogenicity. *Molecules.* 2020;25(23):5698.
47. Akiyama G, Saraswathy S, Bogarin T, et al. Functional, structural, and molecular identification of lymphatic outflow from subconjunctival blebs. *Exp Eye Res.* 2020;196:108049.
48. Lee JY, Heilweil G, Le P, et al. Structural confirmation of lymphatic outflow from subconjunctival blebs of live human subjects. *Ophthalmol Sci.* 2021;1(4):100080.
49. Aguilar-Calvo P, Sevillano AM, Rasool S, et al. Noninvasive antemortem detection of retinal prions by a fluorescent tracer. *J Alzheimers Dis.* 2022;88:1137–1145.
50. Ferreira E, Almeida ZL, Cruz PF, Silva ESM, Veríssimo P, Brito RMM. Searching for the best transthyretin aggregation protocol to study amyloid fibril disruption. *Int J Mol Sci.* 2021;23(1):391.
51. Damrauer SM, Chaudhary K, Cho JH, et al. Association of the v122i hereditary transthyretin amyloidosis genetic variant with heart failure among individuals of African or Hispanic/Latino ancestry. *JAMA.* 2019;322:2191–2202.
52. Spencer-Bonilla G, Njoroge JN, Pearson K, Witteles RM, Aras MA, Alexander KM. Racial and ethnic disparities in transthyretin cardiac amyloidosis. *Curr Cardiovasc Risk Rep.* 2021;15(6):8.
53. Davies DR, Redfield MM, Scott CG, et al. A simple score to identify increased risk of transthyretin amyloid cardiomyopathy in heart failure with preserved ejection fraction. *JAMA Cardiol.* 2022;7:1036–1044.
54. Longhi S, Guidalotti PL, Quarta CC, et al. Identification of TTR-related subclinical amyloidosis with 99mTc-DPD scintigraphy. *JACC Cardiovasc Imaging.* 2014;7:531–532.
55. Mohamed-Salem L, Santos-Mateo JJ, Sanchez-Serna J, et al. Prevalence of wild type ATTR assessed as myocardial uptake in bone scan in the elderly population. *Int J Cardiol.* 2018;270:192–196.
56. Castano A, Haq M, Narotsky DL, et al. Multicenter study of planar technetium 99m pyrophosphate cardiac imaging: predicting survival for patients with ATTR cardiac amyloidosis. *JAMA Cardiol.* 2016;1:880–889.
57. Bokhari S, Castaño A, Pozniakoff T, Deslisle S, Latif F, Maurer MS. (99m)Tc-pyrophosphate scintigraphy for differentiating light-chain cardiac amyloidosis from the transthyretin-related familial and senile cardiac amyloidoses. *Circ Cardiovasc Imaging.* 2013;6:195–201.
58. Papoutsidakis N, Miller EJ, Rodonski A, Jacoby D. Time course of common clinical manifestations in patients with transthyretin cardiac amyloidosis: delay from symptom onset to diagnosis. *J Card Fail.* 2018;24:131–133.
59. Milandri A, Farioli A, Gagliardi C, et al. Carpal tunnel syndrome in cardiac amyloidosis: implications for early diagnosis and prognostic role across the spectrum of aetiologies. *Eur J Heart Fail.* 2020;22:507–515.
60. Boyle RP, Sharan J, Schwartz G. Carpal tunnel syndrome in transthyretin cardiac amyloidosis: implications and protocol for diagnosis and treatment. *Cureus.* 2021;13(4):e14546.
61. Fosbøl EL, Rørth R, Leicht BP, et al. Association of carpal tunnel syndrome with amyloidosis, heart failure, and adverse cardiovascular outcomes. *J Am Coll Cardiol.* 2019;74:15–23.
62. Quarta CC, Gonzalez-Lopez E, Gilbertson JA, et al. Diagnostic sensitivity of abdominal fat aspiration in cardiac amyloidosis. *Eur Heart J.* 2017;38:1905–1908.
63. Cohen OC, Sharpley F, Gilbertson JA, et al. The value of screening biopsies in light-chain (AL) and transthyretin (ATTR) amyloidosis. *Eur J Haematol.* 2020;105:352–356.
64. Ehrlich JR, Ndukwe T, Solway E, et al. Self-reported eye care use among US adults aged 50 to 80 years. *JAMA Ophthalmol.* 2019;137:1061–1066.
65. Bazargan M, Ekwegh T, Cobb S, Adinkrah E, Assari S. Eye Examination recency among African American older adults with chronic medical conditions. *Healthcare (Basel).* 2020;8(2):94.
66. Lee CS, Morris A, Van Gelder RN, Lee AY. Evaluating access to eye care in the contiguous United States by calculated driving time in the United States Medicare population. *Ophthalmology.* 2016;123:2456–2461.